Journal of Aerosol Science 127 (2019) 1–17

Contents lists available at ScienceDirect

Journal of Aerosol Science

journal homepage: www.elsevier.com/locate/jaerosci

Experimental study of drop shape and wake effects on particle scavenging for non-evaporating drops using ultrasonic levitation

S. Fredericks, J.R. Saylor*

Department of Mechanical Engineering, Clemson University, Clemson, SC 29634-0921, USA

ARTICLE INFO

Keywords:
Scavenging
Drops
Shape
Wake
Oscillation

ABSTRACT

Single drop particle scavenging was experimentally measured for a non-evaporating drop using an ultrasonic levitation technique. This technique enabled measurements of scavenging efficiency, E, for individual drops, and allowed for control of drop axis ratio, α, drop shape oscillations, and Reynolds number, Re, independently from drop diameter. Non-evaporating drops were used which resulted in essentially zero temperature and vapor concentration difference between the drop surface and the surrounding air, virtually eliminating the possibility of confounding phoretic effects. Plots of E versus Stokes number, Stk, became independent of α when Stk was calculated using the Sauter mean diameter (as opposed to the equivolume diameter). Furthermore, E was shown to be insensitive to both Re and drop shape oscillations, suggesting that wake effects do not have a measurable impact on E. Finally, a method was developed to relate E for spherical drops, which are assumed for existing scavenging model predictions, to E for arbitrarily deformed drops, such as those occurring in rain. Of note, these are the first measurements of droplet scavenging using ultrasonic levitation.

1. Introduction

Aerosols have been shown to have numerous health (Davis, Bell, & Fletcher, 2002; Docker & Pope, 1994; Pope et al., 1995; Schwartz & Dockery, 1992; Schwartz, 1994; Schwartz, Laden, & Zanobetti, 2002; Seaton, MacNee, Donaldson, & Godden, 1995) and environmental (Horvath, 1993; Kanakidou et al., 2005; Pruppacher & Klett, 1978; Ramanathan, Crutzen, Kiehl, & Rosenfeld, 2001) impacts, making an understanding of their production and removal important to both epidemiology and atmospheric science. Since the concentration of aerosols in the atmosphere affects climate, climate prediction requires models of aerosol removal mechanisms, as well as an understanding of the accuracy of these models (Adams & Seinfeld, 2002; Roeckner et al., 2003; Wang et al., 2010; Webster & Thomson, 2014). One method by which aerosols are removed is through wet scavenging, which is the removal of aerosols by water drops in the atmosphere and is quantified by the scavenging efficiency, defined as:

$$E = \frac{n_c}{n_t} \tag{1}$$

where n_c is the number of particles an individual drop collects and n_t is the total number of particles that the drop could potentially remove as it falls. Models for E are critical to the applications cited above.

Several models exist for prediction of E. These models divide scavenging into several scavenging mechanisms which are modeled separately. The net scavenging is then determined by summing each mechanism's contribution, implicitly assuming that the

* Corresponding author.
E-mail address: jsaylor@clemson.edu (J.R. Saylor).

https://doi.org/10.1016/j.jaerosci.2018.10.001
Received 6 April 2018; Received in revised form 29 August 2018; Accepted 1 October 2018
Available online 11 October 2018
0021-8502/

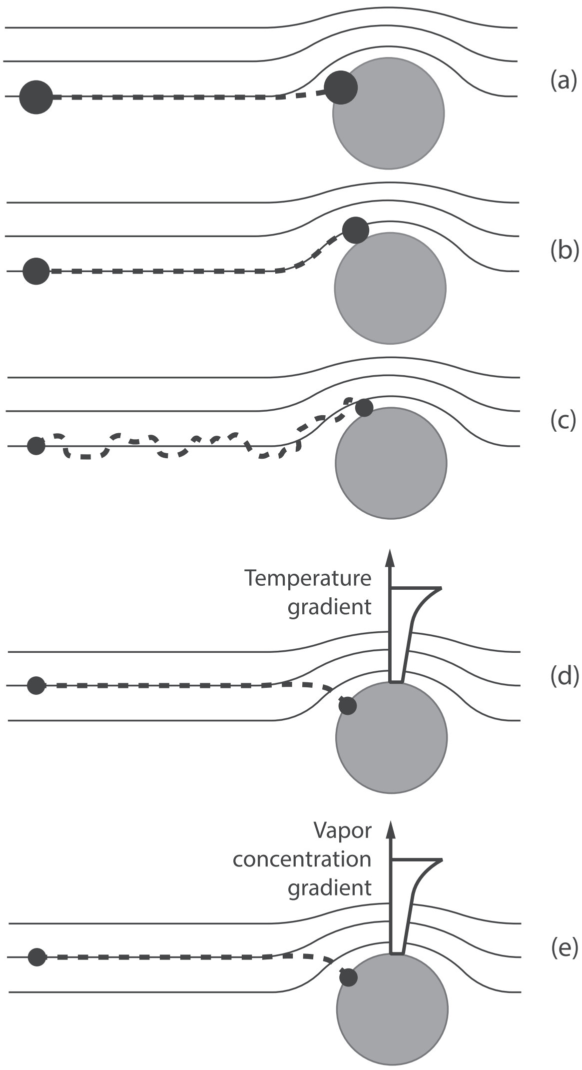

Fig. 1. Schematic showing modes of particle scavenging by drops: (a) inertial impaction, (b) interception, (c) diffusion (Brownian motion), (d) thermophoresis due to a temperature gradient usually caused by drop evaporation, and (e) diffusiophoresis due to a vapor concentration gradient usually caused by drop evaporation.

scavenging mechanisms act independently of each other. The primary modes of particle scavenging by drops are inertial, interception, diffusion, diffusiophoresis, and thermophoresis. Inertial scavenging occurs when the particle possesses enough mass to deviate from its streamline and impact the drop surface (Beard & Grover, 1974; Hinds, 1982; Langmuir, 1948; Slinn, 1984). Interception scavenging occurs when the particle's center of mass does not deviate from its streamline, but due to its finite size it contacts the drop surface and is thereby removed (Friedlander, 1977; Hinds, 1982; Slinn, 1984). Diffusion scavenging is caused by the Brownian motion of small particles as they diffuse across a streamline near the drop, causing them to deposit on the drop surface (Hinds, 1982; Levich, 1962; Slinn, 1984). Diffusiophoretic scavenging occurs when there is a concentration gradient of the vapor phase of the drop surrounding the drop, and thermophoretic scavenging occurs when there is a temperature gradient around the drop. These gradients are generally caused by drop evaporation in wet scavenging applications, and are therefore a function of the drop fluid properties and the humidity of the surrounding air. Hinds (1982), Slinn (1984), Slinn and Hales (1971), Davenport and Peters (1978) A schematic illustration showing each of the above scavenging modes is presented in Fig. 1.

Herein, models of the above scavenging mechanisms are obtained as follows. Inertial scavenging, E_I, is quantified using the model of Slinn (1984) which is based on the simulations of sphere collisions by Beard and Grover (1974). The Slinn model was used instead of the Calvert model (Calvert & Englund, 1984; Calvert, 1970) or the modified Slinn model we developed (Fredericks & Saylor, 2016, 2017) since both of those models rely on curve fitting of data obtained under conditions significantly different from those used in obtaining the present data. The Slinn model also predicts scavenging by interception and by diffusion, E_i and E_D, respectively. Thermophoretic scavenging, E_{tph}, was obtained from the model due to Waldman, as reported by Davenport and Peters (1978), and diffusiophoretic scavenging, E_{dph}, was obtained from the model due to Waldman and Schmidt as reported by Davenport and Peters

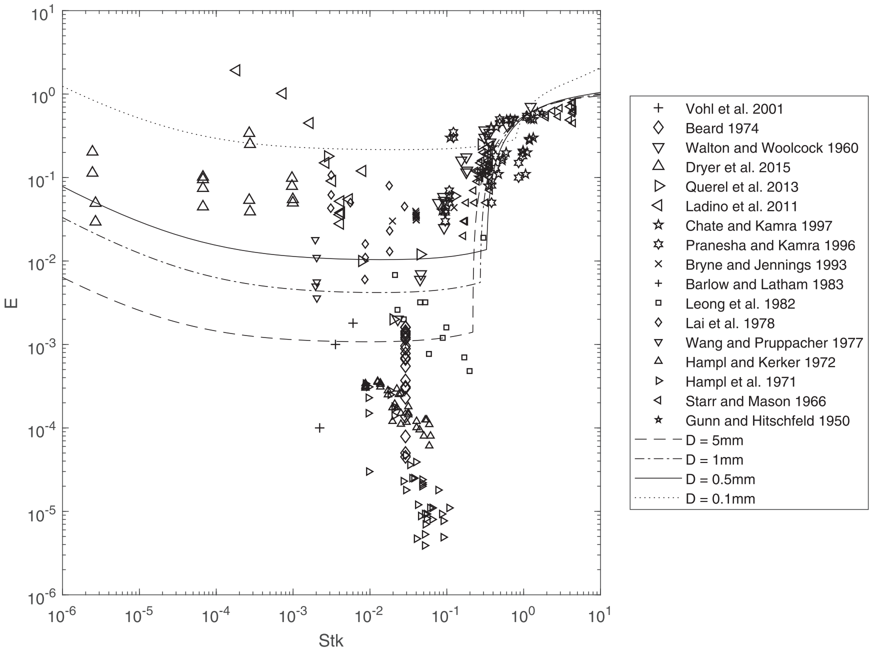

Fig. 2. Plot showing surveyed scavenging data published in the literature (individual points) (Beard, 1974; Vohl et al., 2001; Ladino et al., 2011; Byrne, 1993; Lai et al., 1978; Wang & Pruppacher, 1977; Hampl et al., 1971; Hampl & Kerker, 1972; Ardon-Dryer & Huang, 2015; Quérel et al.,; Chate & Kamra, 1997; Leong et al., 1982; Pranesha & Kamra, 1996; Starr & Mason, 1966; Gunn & Hitschfeld, 1950; Walton & Woolcock, 1960), and the net predicted scavenging from the sum of the models, E_i, E_I, E_D, E_{tph}, and E_{dph}, for various diameter drops at terminal velocity in 50% relative humidity air (lines).

(1978). Expressions for these mechanisms have been reproduced in Appendix A for convenience.

A plot of E versus Stk is presented in Fig. 2, comparing the net scavenging, predicted from the sum of the models described above, along with experimental data published in the literature for single drop scavenging in drop fall towers and vertical wind tunnels (Beard, 1974; Vohl et al., 2001; Ladino et al., 2011; Byrne, 1993; Lai et al., 1978; Wang & Pruppacher, 1977; Hampl et al., 1971; Hampl & Kerker, 1972; Ardon-Dryer & Huang, 2015; Quérel et al.,; Chate & Kamra, 1997; Leong et al., 1982; Pranesha & Kamra, 1996; Starr & Mason, 1966; Gunn & Hitschfeld, 1950; Walton & Woolcock, 1960). While the models for scavenging are functions of several variables, the mechanisms are all typically parameterized in terms of the Stokes number Stk, the abscissa in Fig. 2, which is defined as:

$$Stk = \frac{U\rho d^2 C_c}{9\mu D} \tag{2}$$

where U is the velocity difference between the drop and the particle, ρ is the particle density; D is the drop diameter; d is the particle diameter; μ is the air viscosity; and C_c is the Cunningham correction coefficient:

$$C_c = 1 + \frac{2\lambda}{d}\left[1.257 + 0.4\exp\left(-0.55\frac{d}{\lambda}\right)\right] \tag{3}$$

where λ is the mean free path of air. Note that, unless otherwise stated, the drop diameter D used in the definition of Stk is that of an equivolume sphere. More than one model prediction is presented in Fig. 2 because the models are not solely functions of Stk, and as such will predict different E at a given Stk as the drop diameter changes. In Fig. 2, model predictions are given for drop diameters D= 0.1, 0.5, 1.0, and 5 mm. Also, since phoretic forces will depend on humidity, the predictions in Fig. 2 will change with humidity; the plots presented there are all for water drops in 50% relative humidity. Fig. 2 clearly reveals very large deviations of the data from predictions provided by the models described above. While some of this deviation can be attributed to the model predictions not having been calculated at the same conditions as the experimental data, this accounts for only part of the discrepancy, as we have shown previously (Fredericks & Saylor, 2016, 2017). The cause of most of these deviations is unclear. One possible contributor to the deviations of experimental data from the models of particle scavenging by drops is the fact that the models presume a spherical drop shape, while falling drops attain an oblate shape due to aerodynamic forces and gravity. Furthermore, falling drops oscillate about an equilibrium shape as they fall. Finally, drops can have a wake, depending on their Reynolds number, and this wake can be attached or exhibit vortex shedding; the vortex shedding in turn can potentially couple to drop shape oscillations. All of this is not accounted for in the models of particle scavenging described above. The goal of the present work is to determine if, and to what degree, the above characteristics of falling drops might contribute to deviations of experimental data from model predictions. It should be noted that charging (Beard, 1974) and turbulent diffusion (Wang, Zhang, & Moran, 2011) have been proposed as additional mechanisms which can cause these deviations, however turbulence cannot account for these deviations, as the data presented in Fig. 2 was collected with either drops in the laminar section of a vertical wind tunnel, or for single drops falling though quiescent fluid. Additionally charge neutralization was used in the majority of the data in this figure, therefore charging cannot account for these deviations either.

The deformation of a drop is measured by the axis ratio:

$$\alpha = \frac{v}{h} \tag{4}$$

where h and v are the horizontal and vertical radii of the drop, respectively; for a sphere $\alpha = 1$. This deformation becomes significant for drops where $D > 1$ mm, since the surface tension of water renders deviations from sphericity minimal below this diameter. The $D > 1$ mm diameter range comprises a significant fraction of raindrops. For example, using the Marshall-Palmer (Marshall & Palmer, 1948) drop size distribution at a rain rate of 10 mm/h, 28% of drops will be larger than 1 mm, and 73% of the mass of rain falls in this $D > 1$ mm range. Drop deformation increases with D. For example a 1 mm, 2 mm, and 3 mm drop will be deformed to α= 0.98, 0.93, and 0.86, respectively, under equilibrium conditions. Beard (1976), Andsager, Beard, and Laird (1999)

As noted above, wakes can exist in the flow behind the drop. The wake is primarily determined by the drop Reynolds number:

$$Re = \frac{\rho_a UD}{2\mu} \tag{5}$$

where ρ_a is the air density (note that drop radius is the characteristic length in Eq. (5)). For spheres, an attached wake appears at $Re \sim 100$, and vortex shedding begins at $Re \sim 300$ (Sakamoto & Haniu, 1990). This wake behavior has been observed in simulated raindrops with diameters between 1.65 and 2.91 mm (Saylor & Jones, 2005). For raindrops falling at their terminal velocity, as determined by the terminal velocity equation due to Beard (1976), Re will be sufficiently large to form an attached wake for drops larger than 0.6 mm, and for drops larger than 1.1 mm Re will be large enough for vortex shedding to occur. Applying this to the Marshall-Palmer distribution for 10 mm/h rain, this corresponds to 75% of raindrops having a wake, and 23% of drops experiencing vortex shedding. Additionally, a drop will not have a stationary shape as it falls, and will instead oscillate about its equilibrium shape, having a change in α throughout its oscillation cycle on the order of 0.02 (Andsager et al., 1999; Tokay & Beard, 1996) and these shape oscillations can be coupled to the vortex shedding of the drop wake (Beard, Ochs, & Kubesh, 1989), as noted above.

Of the data presented in Fig. 2, the majority of the experiments were for drops where Re was in the range where a wake is expected, however none of these works investigated the role of wakes in detail. Additionally, some of these experiments had drops large enough to exhibit deformation, however this is the minority of experiments and the role of α on E was not investigated. Finally, although the experiments with drops large enough to exhibit deformation will also exhibit oscillation, none of these experiments explored the role of drop oscillation on scavenging. Hence, since drop deformations, wakes, and drop shape oscillations all can exist in falling drops, but their influence on scavenging has not been quantified in the existing analytical or experimental literature, a new scavenging measurement method was developed to quantify these effects. This method used an acoustically levitated drop which can easily be exposed to aerosol laden flows. This approach differs from the previously used scavenging measurement techniques of fall towers and vertical wind tunnels in that U and the drop axis ratio, α, can both be adjusted independently of D, which is not the case for a freely falling drop (Andsager et al., 1999; Beard & Chuang, 1987; Beard, 1976). The drop velocity and shape combine to determine Re, which can classify the wake size (Zamyshlyaev & Shrager, 2004) and vortex shedding of the wake (Sakamoto & Haniu, 1990). Previously we have shown that model residuals with the existing published scavenging values correlate well with Re, which we hypothesized might be due to wake effects. This will be explored in more detail using the ultrasonic levitation method, herein. Additionally this method can be used to induce shape oscillations in the drop, and the magnitude of these oscillations can be independently controlled, allowing this effect to be exaggerated to more clearly determine if it affects scavenging. Therefore the significance to scavenging of static and dynamic drop shape and drop wake can be evaluated.

Finally, it is noted that the experiments presented in Fig. 2 were all conducted for water drops in unsaturated conditions. In such a situation evaporation can cause concentration gradients which leads to diffusiophoretic effects, as well as evaporative cooling of the drop surface, leading to thermophoretic effects. In the experiments presented below, propylene glycol was used instead of the more typical water to minimize the evaporation of the drop during these tests. This approach minimizes phoretic scavenging contributions, which may otherwise dominate effects due to shape deformation, shape oscillations, and wakes.

2. Experimental method

An ultrasonic standing wave field was used to levitate a stationary drop within a particle laden jet. Unlike fall tower and wind tunnel experiments which have traditionally been used in drop scavenging experiments, this approach allowed for control of drop shape independent from drop diameter, and easily allowed for exploration of both sub-terminal and super-terminal velocities. The apparatus used is shown in Fig. 3.

Ultrasonic levitation involves the development of an acoustic standing wave field. At the nodes of such a field, the acoustic radiation force will support an object (Danilov & Mironov, 2000; Karlsen & Bruus, 2015; King, 1934; Merrell & Saylor, 2016; Ran, Saylor, & Holt, 2014; Settnes & Bruus, 2012). The ultrasonic standing wave field supporting the drop was created using an ultrasonic transducer, a reflector, a function generator, an amplifier, and custom control software. The transducer consisted of two piezoelectric disks with a copper plate between them, an aluminum back mass, and an emitter, following the design of Trinh (1985). To drive the transducer an Agilent 33220A function generator was used to generate a sine wave at the resonant frequency of the transducer/reflector system, approximately 30 kHz, with a peak to peak amplitude of 300–900 mV. The function generator output was amplified

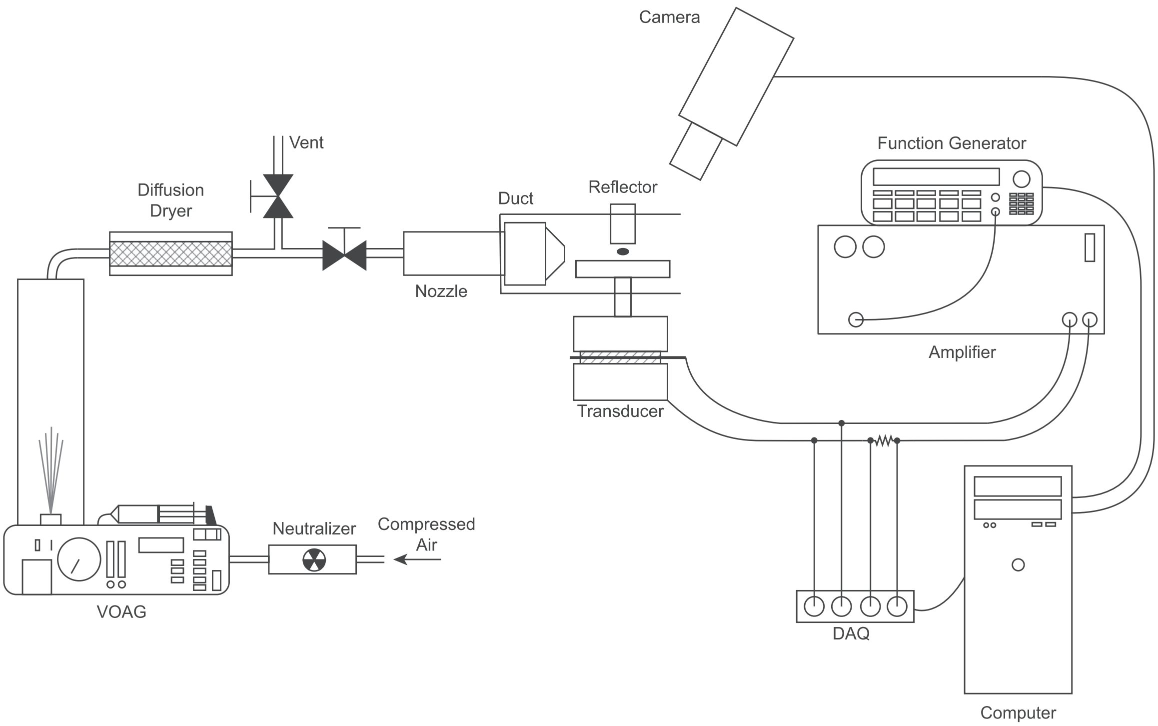

Fig. 3. Diagram of the experimental apparatus used to determine the scavenging coefficient of individual drops.

using a Krohn-Hite 7500 amplifier to produce a signal of 30–90 V which was applied to the ultrasonic transducer. The transducer, thus driven, emitted a nominally planar wave which was reflected by the reflector, consisting of a flat aluminum surface placed an integer number of half wave lengths from the transducer. This produced the ultrasonic standing wave field used to levitate droplets in the experiment.

The resonance frequency of the transducer was found to drift with time as the transducer was operated. To account for this, a software control was implemented in LabView. To ensure that the applied signal was at the resonant frequency of the transducer/reflector system, the applied voltage and current were measured with a Measurements Computing USB-2020 DAC at a sample rate of 10 MHz. The phase shift between the voltage and current was calculated, and the driving frequency was subsequently adjusted to reduce the phase shift to zero, maximizing the power delivered to the transducer. This change in frequency resulted in a change in wavelength of the ultrasonic wave, and as the gap between the reflector and transducer is fixed, this process therefore detuned the ultrasonic wave field to no longer be a pure standing wave. This change in the reflector gap tuning is very small, on the order of microns and microns and had far less impact on our ability to levitate drops than keeping the frequency constant and not compensating for the drift in the transducer resonance frequency. This method allowed a droplet to be levitated for several hours, which is significantly longer than the duration of a typical scavenging experiment.

With a drop floating in the field, the drop shape was adjusted by changing the voltage applied to the transducer. Increasing the applied voltage resulted in more oblate drops while decreasing the field resulted in more spherical drops. Images of the levitated drop were obtained during each experiment using a Cooke Sensicam high speed camera, and were used to measure drop diameter. An example drop image is shown in Fig. 4. A Canny edge detection algorithm (Canny, 1986) was applied to the image and the horizontal and vertical extents of the drop were found, giving the major and minor radii of the drop, h and v respectively, which were used to obtain α as defined in Eq. (4). The three dimensional shape of the drop was assumed to be an oblate spheroid where the equivolume spherical diameter,

$$D = 2h\alpha^{1/3} \tag{6}$$

was used to quantify the drop size. During stationary drop tests the field strength was kept constant and the drop shape was not observed to change.

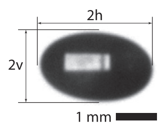

Fig. 4. Back lit image of a levitated drop, with the light visible through the drop.

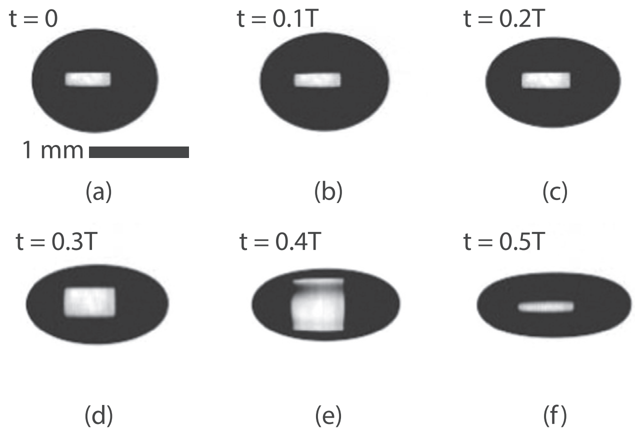

Fig. 5. Back lit images of a levitated drop undergoing oscillation, beginning at (a) with the largest α indicating the smallest field strength, then progressing sequentially through the first half of the oscillation period, T, (b), (c), (d), and (e) showing intermediate drop shapes, and (f) showing the smallest α indicating the largest field strength. As the oscillation is periodic in time, only the first half of the oscillation period is presented.

It should be noted that while the above method produces an oblate spheroid, which is the shape a raindrop will achieve as it falls, the direction of the flow relative to the minor axis of the drop is orthogonal to the flow condition in rain. This deviation from the natural condition of rain notwithstanding, this approach is useful because it allows for us to independently control the drop Reynolds number, shape, and oscillations, which are all typically determined by the drop diameter. By decoupling these parameters, this method allows us to more easily explore the impact of these parameters independently, and pinpoint their influence on scavenging. Additionally, a method was developed to account for the change in drop orientation relative to that of a freely falling droplet, as is described in the Discussion.

To induce drop oscillations, the signal applied to the transducer was amplitude modulated (AM) causing the drop to oscillate at the AM frequency. An example series of back lit drop images is presented in Fig. 5 which shows the shape of the drop through half of an oscillation period. For the oscillating drop tests, the mean α was used to classify the drop shape, and the equivolume spherical diameter was used to calculate Stk. Modulation frequencies were applied at both the drop natural frequency as described by Lamb (1932) and at the frequency which produced the largest amplitude oscillations, which was typically approximately half the frequency predicted by Lamb. In this work, these frequencies ranged from 60 to 100 Hz. That the larger amplitude oscillations were observed to occur below the Lamb frequency is likely due to the non-spherical shape of the drops in this experiment. Shen et al. have shown that there is a decrease in the frequency of sectoral oscillations in an oblate drop with increasing drop deformation (Shen, Xie, & Wei, 2010a, 2010b), so it stands to reason that a similar dependence would hold for oblate-prolate oscillations. Additionally Trinh and Wang have shown that for large amplitude, driven oscillations, such as those in this experiment, the observed peak in oscillation amplitude is dependent on the degree of modulation of the ultrasonic field (Trinh & Wang, 1982), indicating that some shift from the Lamb frequency should be expected. In both oscillating cases the jet velocity was adjusted so that the vortex shedding frequency, as predicted by Sakamoto and Haniu (1990), was an integer multiple of the imposed drop oscillation frequency.

Propylene glycol was used as the drop fluid in these experiments to minimize change in the drop size due to evaporation over the course of the experiments. Initial runs conducted with water as the working fluid resulted in significant changes in drop diameter over the course of an experiment. For example, over ten minutes a 91% reduction in drop volume was observed for water. This corresponds to a 55% reduction in drop diameter. By using the relatively nonvolatile propylene glycol the drop volume only decreased by 7% in the same duration, which corresponds to only a 2% reduction in diameter. This allowed for longer runs, which collected more total particles, therefore increasing the signal measurement and reducing the uncertainty in E, without introducing confounding effects due to changing D through the course of the run. This approach had the added benefit of essentially removing phoretic effects, which may otherwise mask the influence of drop shape, wake, and oscillations which is the goal herein.

To produce monodisperse particles, a vibrating orifice aerosol generator (TSI 3450 VOAG) was used. The VOAG produces monodisperse droplets by exciting a liquid jet, thereby causing the jet to break up into a stream of monodisperse droplets. The jet is composed of a solution containing a nonvolatile solute (a dye), and the resulting monodisperse droplets evaporate, producing a monodisperse aerosol with the particle diameter controlled primarily by the concentration of the dye according to Berglund and Liu (1973):

$$d = \left(\frac{6QC}{\pi f}\right)^{1/3} \tag{7}$$

where Q is the VOAG solution flowrate, C is the dye volume concentration, and f is the vibration frequency of the VOAG. Disodium fluorescein was chosen as the dye because it is a well characterized fluorescent dye, which fluoresces when excited by ultraviolet light. It has a peak excitation wavelength of 480 nm and a peak emission wavelength of 525 nm (Saylor, 1995). The intensity of the emitted light depends on the intensity of the absorbed light, the dye concentration, and the solution pH (Ohkuma & Poole, 1978).

Taking advantage of this response, a fluorometer (Turner Designs, PicoFlour 8000–003) was used to measure the concentration of the sample, which in turn was used to determine the mass, or number of particles present, in the sample.

The air entering the VOAG was first directed through a krypton 85 neutralizer (TSI 2077A) to remove charge from the generated particles so that any electrostatic attraction could be assumed negligible between particles or between particles and drops. The particles were then transported through a diffusion dryer to ensure that the particles were entirely dry. Following the diffusion dryer the flow exited via a nozzle based on the design of Bell and Mehta (1988), which produced a uniform velocity particle laden jet. The particle concentration was determined by clamping a 3 µm Teflon filter (Millipore) over the nozzle outlet for 1 min to collect particles. This filter was then removed, washed with 10 ml doubly distilled water, and 40 μl of the resulting solution was transferred to a cuvette containing 40 μl of 10 pH buffer solution. The resulting solution was then measured with a fluorometer to determine the concentration of disodium fluorescein particles in the jet. Drops were typically levitated in the particle laden jet flow for 5–20 min at which time the drop exhibited visible color change. At this time the drop was then removed from the field and mixed with 0.2 ml of 10 pH buffer solution. The resulting solution was measured with a fluorometer to determine the amount of disodium fluorescein collected by the drop. Using these two measurements, the scavenging coefficient was determined according to the equation:

$$E = \frac{f_d V_d t_f A_j}{f_f V_f t_d A_d} \tag{8}$$

where f_d and f_f are the disodium fluorescein concentrations for the drop and filter respectively, V_d and V_f are the dilution volumes for the drop and filter respectively, t_f and t_d are the duration of the filter test and drop exposure respectively, and A_j and A_d are the cross sectional area of the jet and the projected area of the drop respectively.

The above experimental method produces E which can exceed unity, a violation of conservation of mass. This increased scavenging is due to three artifacts in the experimental method which yield artificially high E. The first contributor is a decrease in flowrate through the system when the filter was mounted relative to the flowrate when the drop was exposed to the jet. For large particle diameter d, this drop in flowrate caused additional particle settling in the particle generator and a decrease in the mass collected by the filter, resulting in under-counting of the fluorescein concentration in the jet. The second artifact is due to the ultrasonic field, which compresses the particle trajectories as they travel from the nozzle to the drop. Just as the acoustic radiation force compresses the drop in the node of the standing wave field, so too are the particles pushed toward the node, although this compression of particle trajectories is much smaller than the degree to which the drop is compressed. This results in a larger fluorescein concentration in the region of the field near the drop than is measured by the filter. The third artifact was a change in the tube geometry between the diffusion dryer and the nozzle when the nozzle was moved for the filter collection portion of the experiments which resulted in increased deposition in the tubing, resulting in an under counting of the fluorescein concentration of the jet the drop was exposed to.

These three contributors were corrected to provide the actual E presented in the Results section, below. To correct for the drop in flowrate during the filter collection, experiments were conducted to measure filter collection at the actual flow rate of each experiment. Compression of particle trajectories in the ultrasonic standing wave field was accounted for by simulating the particle trajectories as they travel from the nozzle to the drop. The acoustic radiation force exerted by the acoustic field on the particles was calculated using the formulation due to Settnes and Bruus (2012), and the drag experienced by the particles was calculated as Stokes drag. A correction factor was created from these simulations by taking the ratio of the particle concentration at the nozzle exit and at the drop location. Further details on the calculation of this correction factor are presented in the online supplemental materials. Finally the increased deposition in the tubing during the filter collection due to different tube bend geometry upstream of the nozzle was accounted for using the tube deposition model due to McFarland, Gong, Muyshondt, Wente, and Anand (1997).

3. Results

A plot of E versus Stk is presented in Fig. 6, where E is the corrected scavenging coefficient, as described above, and Stk is computed using the diameter of an equivolume sphere (Eq. (6)) for the length scale in Eq. (2). An E versus Stk plot for the uncorrected data can be found in the online supplemental material. The value of α for each data point is indicated via grayscale. These data show that E increases monotonically with Stk, for the range of Stk explored here. Also, for a given Stk, E increases with decreasing α (E increases as the drops become less spherical). This trend with α becomes more pronounced for smaller Stk. This is seen more clearly when the data is binned in Stokes space and E is plotted against α within the Stk bin, as shown in Fig. 7. This figure shows, again, that E decreases with α, and that this decrease is largest for small Stk.

To see how Re, and therefore wake effects, influence E the data from Fig. 6 was binned evenly in Stk and plotted against Re, where the length scale in Re was the drop minor diameter. A series of E versus Re plots were obtained, similar to those presented in Fig. 7, which showed essentially no sensitivity of E to Re. The Reynolds number ranged from $Re = 100 - 500$, which includes both the attached wake and the vortex shedding wake regimes (Sakamoto & Haniu, 1990). To further demonstrate the insensitivity of E to Re, the data within each Stk bin was fit to an exponential function of the form:

$$E = Ce^{(\phi_{Re})(Re)} \tag{9}$$

so that the exponent ϕ_{Re} quantifies the sensitivity of E to Re. This exponent is plotted against the average Stk for each Stk bin in Fig. 8. As the figure shows, $\phi_{Re} = 0$ within the 95% confidence intervals of the data, further demonstrating that E is insensitive to Re. This suggests that wake effects are not playing a measurable role in scavenging, though it should be noted that for $Stk < 0.6$, the 95%

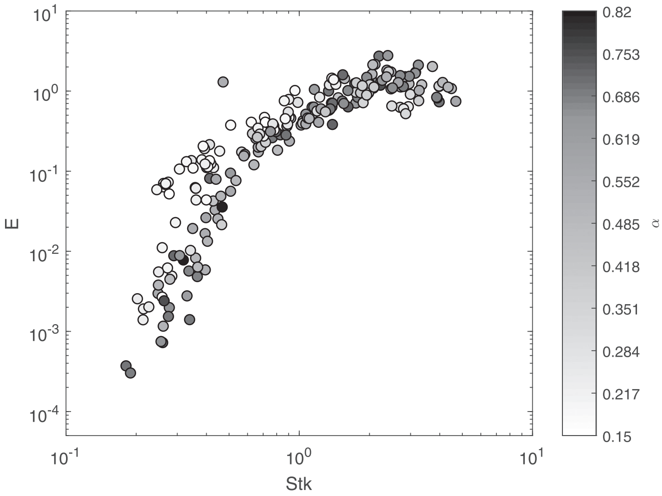

Fig. 6. Plot of scavenging coefficient, E, versus Stokes number, Stk, where Stk is based on the equivalent volume spherical diameter of the drop. The marker grayscale intensity indicates the drop axis ratio, α for each data point. These data are for stationary drops.

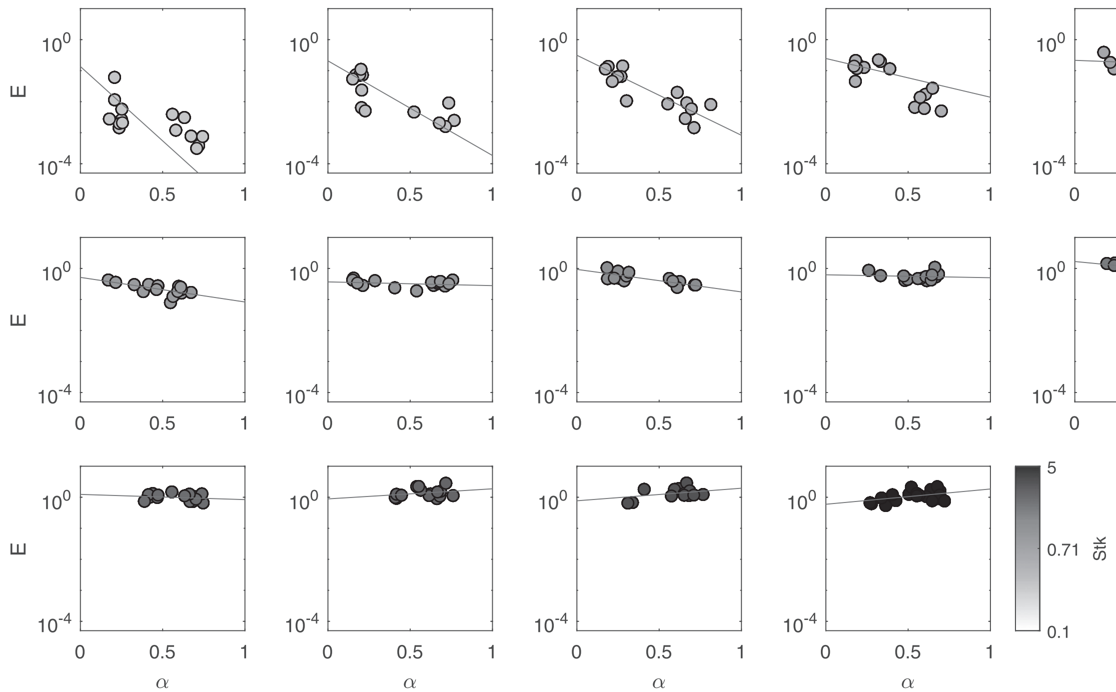

Fig. 7. Plots of scavenging coefficient E versus drop axis ratio α, for stationary drops. Each plot is for a fixed range of Stk. The Stokes number increases from left to right and top to bottom encompassing the entirety of the data in Fig. 6, binned evenly in Stk. The Stk bins are: (0.182:0.263); (0.263:0.308); (0.308:0.363); (0.363:0.415); (0.416:0.511); (0.511:0.699); (0.699:0.812); (0.812:1.025); (1.025:1.302); (1.302:1.546); (1.546:1.931); (1.931:2.209); (2.209:4.719). The Stokes number for each data point is indicated by grayscale.

confidence intervals are large. Hence, it is possible that there is some sensitivity to Re in this range that the data is unable to reveal. It is noted that this insensitivity to Re holds true for drops in the attached wake regime and drops in the vortex shedding regime.

In addition to the stationary drop scavenging measurements presented in Fig. 6, measurements were made while acoustically inducing oscillations in the drops. These drop oscillations were excited at both the natural frequency predicted by Lamb (1932) as well as the frequency which gave the largest change in α for a given field strength. For all oscillating drops the jet velocity was adjusted so that the vortex shedding frequency, as predicted by the Strouhal number measurements of Sakamoto and Haniu (1990) for a sphere, was 4 times the drop oscillation frequency, meaning that a second harmonic coupling between vortex shedding and drop oscillation was attained. Fig. 9 shows the binned, non-oscillating measurements from Fig. 6 as well as E for the oscillating drops. The degree of oscillation is quantified by $\Delta\alpha$ the difference between the maximum and minimum α during the oscillation cycle and is

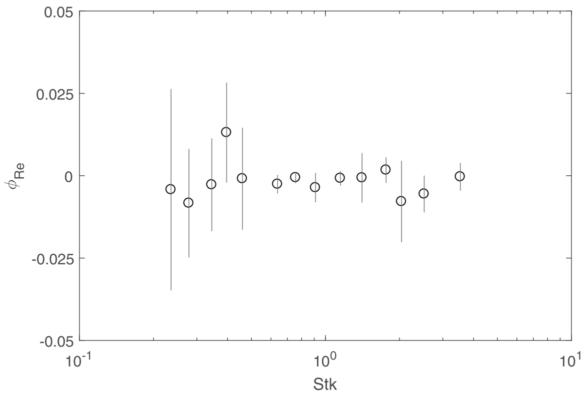

Fig. 8. Plot showing the sensitivity of E to Re as a function of Stk based on E versus Re fits of the data in Fig. 7 binned in Stk. The vertical bars show the 95% confidence intervals of ϕ_{Re}.

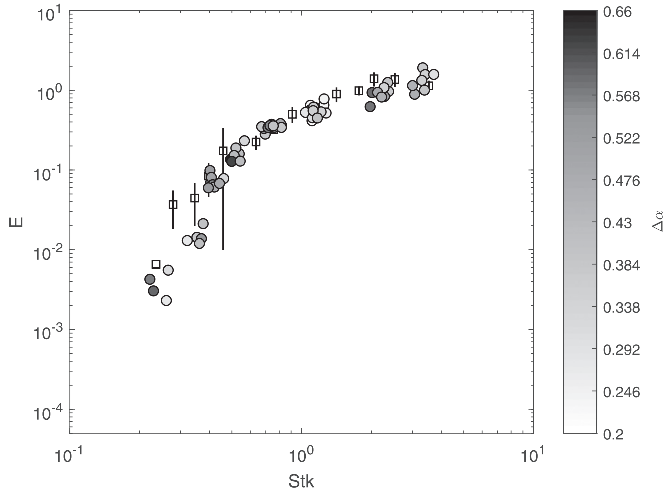

Fig. 9. Plot of the bin average of the non-oscillating data (squares) from Fig. 6 and the oscillating drop measurements (circles). For the oscillating data the grayscale value indicates the magnitude of the drop oscillations as measured by the difference between the maximum and minimum α of the oscillation cycle, $\Delta\alpha$. The vertical bars show the 95% confidence interval of the non-oscillating drop bins.

indicated via grayscale in Fig. 9. As this figure shows, the oscillating scavenging measurements appear to be insensitive to the degree of oscillation, which is larger in all cases than that of a freely falling raindrop (Andsager et al., 1999). The oscillating data also does not deviate from the non-oscillating data within the confidence intervals. All this indicates that drop oscillations do not materially contribute to scavenging.

4. Discussion

An important result presented above is the increase in E with decreasing α shown in Figs. 6 and 7, which occurs at small Stk. This result can be explained by considering how the drop surface area and projected area change with α. For a fixed volume drop in the flow conditions of this experiment (where α is always <1) the surface area decreases with increasing α, while the projected area increases with increasing α. This leads to a situation where there is more area available for particles to deposit at small α, while simultaneously decreasing the number of particles in the flow path of the drop. This can explain the observed increase in scavenging for small α and Stk, where the scavenging contribution is dominated by surface area dependent mechanisms such as diffusional deposition, and phoretic forces. However, at large Stk, inertia becomes dominant, which is a projected-area-dependent mechanism. For this case both the number of particles encountering the drop and the removal of particles by the drop are determined from the projected area. Since E is a ratio of these two values, large Stk scavenging should therefore be independent of α, which is in fact the case, as Figs. 6 and 7 show.

The above explanation can be shown more formally with the following scaling argument, similar to the method used by Slinn and Hales (1971). First, the rate a drop is exposed to particles, $\dot{n}_t$, is assumed to scale as:

$$\dot{n}_t \sim n_\infty U A_d \tag{10}$$

where n_∞ is the freestream particle concentration and A_d is the projected area of the drop. Also, it is assumed that the drop collects these particles at the rate $\dot{n}_c$, which is given by the relationship:

$$\dot{n}_c \sim \Gamma A \tag{11}$$

where Γ is the net flux, in particles per time per area, of particles moving from the air to the drop at the drop surface due to all scavenging mechanisms, which is assumed to be independent of drop shape, and A is the area of the drop surface which is interacting with the particles, and is dependent on drop shape, α. For large Stk, where inertia is dominant, $A = A_d$, but for smaller Stk, $A = A_S$, where A_S is the drop surface area. The ratio of $\dot{n}_c$ to $\dot{n}_t$ gives E, so for large Stk E will scale as:

$$E \sim \frac{\Gamma A_d}{n_\infty U A_d} = \frac{\Gamma}{n_\infty U} \tag{12}$$

and E is insensitive to drop shape, while for small Stk E will scale as:

$$E \sim \frac{\Gamma A_s}{n_\infty U A_d} \tag{13}$$

which is a function of α, and E will increase as α decreases. These large and small Stk relations agree with the experimental observations.

The above relationship can be used to relate scavenging for a sphere, E_s, with scavenging for an oblate spheroid (such as the data herein), E_o. This is accomplished by substituting expressions for the surface and cross sectional areas of oblate spheroids and spheres into Eq. (13), and taking the ratio of E_s and E_o, which gives the relationship:

$$\frac{E_s}{E_o} = \frac{2\alpha}{1 + \frac{\alpha^2}{\sqrt{1-\alpha^2}}\tanh^{-1}(\sqrt{1-\alpha^2})} \tag{14}$$

This can be expanded further to predict how an oblate spheroid will scale with the measured Stk in the present study, which will allow for quantifying the influence of the drop shape in the scavenging results. This is done by making the following assumptions. First, that E primarily scales with the Stokes number, and second that the Stokes number characteristic length for an oblate spheroid, Stk_o, is the major diameter, which can be related to the equivolume spherical Stokes number (Stk) according to:

$$\frac{Stk}{Stk_o} = \alpha^{1/3}. \tag{15}$$

By combining Eqs. (14) and (15) the following relationship is obtained:

$$E_o \sim Stk\left[\frac{1 + \frac{\alpha^2}{\sqrt{1-\alpha^2}}\tanh^{-1}(\sqrt{1-\alpha^2})}{2\alpha^{2/3}}\right] \tag{16}$$

Eq. (16) show that the scavenging of an oblate spheroid, such as a falling drop, is a function of Stk and α, and scales directly with Stk. An important result is that multiplying Stk by the portion of Eq. (16) in square brackets yields the Stokes number using the Sauter mean diameter, D_S, as the characteristic length for the drop, where:

$$D_S = 6\frac{V}{A_s} \tag{17}$$

where V is the drop volume, and A_s is the drop surface area. Therefore, for deformed drops in the flow conditions of this study, Eq. (16) can be rewritten as:

$$E_o \sim Stk_S \tag{18}$$

where Stk_S is the Sauter mean diameter based Stokes number. To the authors' knowledge this is the first use of D_S as the length scale for Stk. The Sauter mean diameter is the diameter of a sphere which preserves the surface area to volume ratio of an oblate spheroid, and is commonly used in surface area dominated processes (Hinds, 1982). Replotting the data obtained herein against the Sauter mean diameter based Stokes number, Stk_S, it is seen that E becomes insensitive to α, as shown in Fig. 10. To better visualize this trend this data was binned in Stk_S space and plotted as a function of α, then curve fit to an exponential function of the following form:

$$E = Ce^{(\phi_\alpha)(\alpha)} \tag{19}$$

The resulting ϕ_α are plotted against Stk_S in Fig. 11. The confidence intervals for ϕ_α span zero for all Stk_S indicating that there is no statistically significant sensitivity of E to α. Therefore E for an arbitrarily deformed drop in the flow orientation of the experiment herein can be used to predict the scavenging for a spherical drop, and vice-versa.

Because Stk_S accounts so well for α effects, it can also be used to better understand the oscillating results from this experiment. Recalculating the data from Fig. 9 to be based on Stk_S removes any influence of drop shape on E as discussed above. This highlights any potential dynamic effects in the collected data. Fig. 12 presents the data thus treated, showing the binned, stationary measurements from Fig. 10 as well as the measured oscillating drops. The oscillating data was evaluated at Stk_S for the average α of the oscillation cycle. As this figure shows, the oscillating values agree well with the stationary results. This gives further indication that

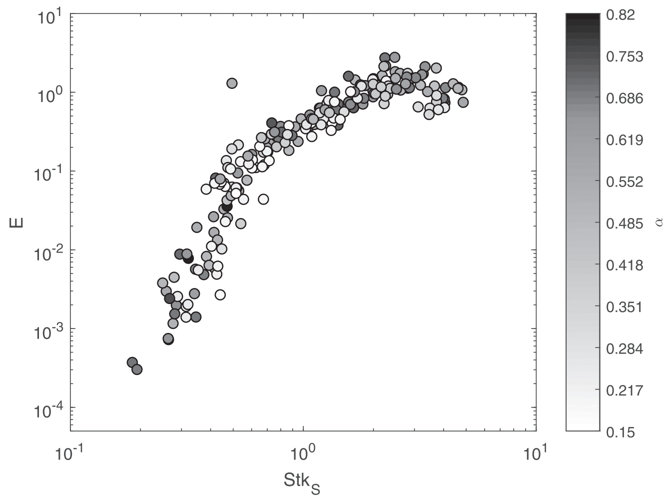

Fig. 10. Plot of the measured scavenging as a function of Stk_S calculated with the Sauter mean diameter for stationary drops.

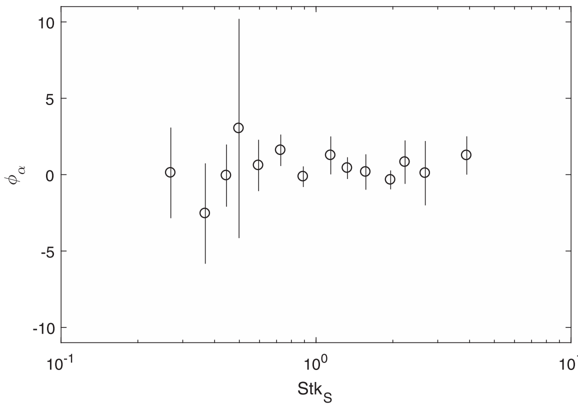

Fig. 11. Plot showing the sensitivity of E to α as a function of Stk_S based on E versus α fits of the data in Fig. 10 binned in Stk_S. The vertical bars show the 95% confidence intervals of ϕ_α.

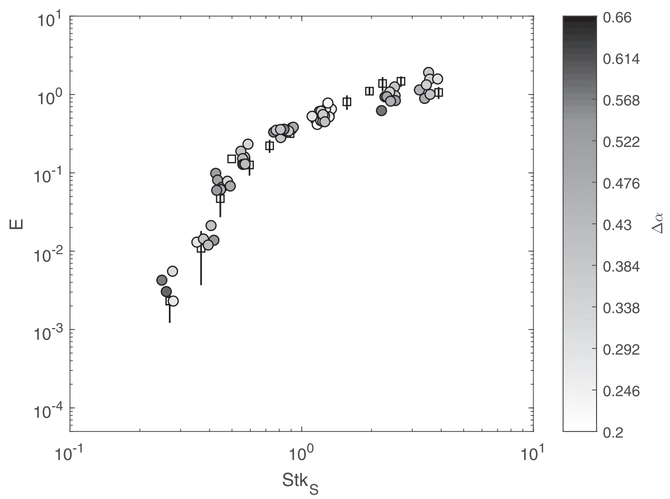

Fig. 12. Plot of the bin average of the non-oscillating data (squares) from Fig. 10 and the oscillating drop measurements (circles). For the oscillating data the grayscale indicates the magnitude of the drop oscillations as measured by $\Delta\alpha$, the difference between the maximum and minimum α of the oscillation cycle. The vertical bars show the 95% confidence interval of the non-oscillating drop bins.

the previous conclusion of E insensitivity to wake effects is valid, as for the exaggerated case tested here there is no measurable discrepancy between the stationary and oscillating drop conditions. As there appears to be no wake effects, the correlation between the model residuals and Re we have identified previously (Fredericks & Saylor, 2016, 2017) must be due to some other Re dependent process which is not present in this experiment. As the drop fluid in this experiment was chosen to have a very low evaporation rate to facilitate longer scavenging durations to minimize uncertainty, and the convective mass and heat transfer from an evaporating drop are both Re dependent, it is likely that phoretic forces are the cause of the Re correlated model residuals found in our prior work. This hypothesis is explored in greater detail later in this Discussion.

As the above analysis has been demonstrated to account for α in the present data, we conclude that the assumptions made in Eqs. (10) and (11) are sufficient to capture the relevant physics of the scavenging process. Recall that the orientation of the drops used in this investigation are rotated perpendicular relative to the flow direction compared to the orientation of a freely falling rain drop. Therefore the results above will not apply directly to rain. However, the same analysis used to obtain Eq. (14) can be applied for the orientation of a raindrop. That is, the ratio can be obtained for the scavenging coefficient for a sphere, E_S, to the scavenging coefficient of an oblate spheroid oriented as raindrops are, E_r. This ratio is:

$$\frac{E_s}{E_r} = \frac{2}{1 + \frac{\alpha^2}{\sqrt{1-\alpha^2}}\tanh^{-1}(\sqrt{1-\alpha^2})} \tag{20}$$

This relationship allows for spherical scavenging models to be used to predict scavenging for arbitrarily deformed rain drops and vice-versa. For example, the scavenging models discussed in the Introduction all assume a spherical drop and by applying Eq. (20) to these model predictions, new predictions can be obtained which account for the deformations present in rain. This will be shown below. Another example of the utility of the analysis presented in Eqs. (14) and (20), is that they can be used to directly compare the present data with that of previous researchers, by converting both sets of measured values to equivalent spherical scavenging measurements. This will be presented later in this Discussion.

As noted in the Introduction, raindrops larger than 1 mm will deform due to aerodynamic forces and gravity. Eq. (20) allows for these drop deformations to be accounted for, and the extent of their influence on particle removal in a rain event to therefore be quantified. The following analysis is an example which demonstrates this by modeling particle removal in two ways: first by assuming the rain drops are spherical and applying the models for E without modification; then by accounting for drop deformation to obtain E_r from the spherical E via Eq. (20). Comparing the net particle removal in both cases quantifies the impact of drop shape on scavenging. To do this, the raindrop size distribution was obtained using the Marshall-Palmer model (Marshall & Palmer, 1948), and the shape of each drop diameter was determined using the relationship due to Andsager et al. (1999):

$$\alpha(D) = 1.0048 + 0.0057D - 2.628D^2 + 3.682D^3 - 1.677D^4 \tag{21}$$

with the units for D in cm. The terminal velocity of each drop diameter was obtained from the model due to Beard (1976). The individual drop E was found using the models described in the Introduction. These models were evaluated in two ways: first for spherical drops with the unmodified models, then accounting for drop deformations by applying Eq. (20) to obtain E_r. The particle size distribution was determined from the model due to Clark and Whitby (1967). Following Slinn (1984), the evolution of the particle concentration during a rain event is:

$$n(d, t) = n(d, 0)e^{-\Lambda(d)t} \tag{22}$$

where n is the particle concentration, t is the rain duration, and Λ is the washout coefficient found by: Slinn (1984)

$$\Lambda(d) = \int \frac{\pi}{4}(D + d)^2 U(D)E(d, D)N(D)dD \tag{23}$$

where N is the drop size distribution. The difference between $n(d, 0)$ and $n(d, t)$ gives the modeled particle removal over the course of the rain event. Applying this analysis results in a decrease in modeled particle removal when accounting for the drop shape compared to the calculated removal for spherical drops. The magnitude of this decrease depends on the rain rate and frequency of rain events, therefore to reveal the significance of this analysis, it is applied in two example cases, a U.S. city that experiences high rainfall, and one that experiences low rainfall. For Orlando, FL, the analysis shows that accounting for α results in a decrease of 11,800,000 kg of particles removed per year over the city, which is a 0.3% decrease in predicted particulate removed. When this is applied to the much drier Las Vegas, NV, the prediction accounting for shape effects results in 1880,000 kg less of particulate removed per year, which is a 0.27% decrease compared with the predicted removal from spherical drops. In both cases the difference is large in terms of mass of particulate removed, but small in terms of percentage.

Because Eqs. (14) and (20) allow for spherical drop scavenging to be extrapolated from arbitrarily deformed drops in both the orientation of the present experiment and of a falling raindrop (which is the orientation for drop fall towers and vertical wind tunnels) respectively, the results of this study can now be readily compared with existing experimental scavenging measurements, as well as scavenging models for spherical drops. Fig. 13 shows how the data collected herein compares with previously published single drop scavenging measurements in the same Stokes range. To account for drop deformations, E has been adjusted to give the spherical drop equivalent scavenging, E_s. To minimize clutter, the results from this study have been binned and the averages plotted. The other data presented in this figure comes from the surveyed single drop scavenging literature with measurements of E for $Stk > 0.1$, which is the range of the present study (Quérel et al., (), Ladino et al., 2011; Chate & Kamra, 1997; Pranesha & Kamra, 1996; Leong, Beard, & Ochs, 1982; Starr and Mason, 1966; Walton & Woolcock, 1960; Gunn & Hitschfeld, 1950).

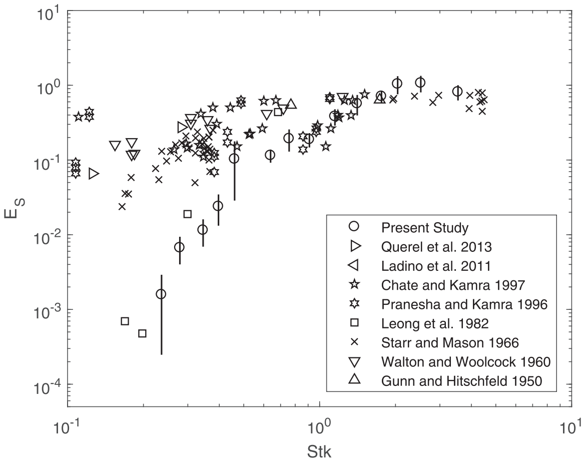

Fig. 13. Plot of present scavenging measurements and previously published scavenging measurements. All measurements have been adjusted to equivalent spherical scavenging via Eq. (14) for the data in the present experiment, and via Eq. (20) for the previously published results. The present results have been binned and averaged for clarity, the error bars show the 95% confidence bounds of the averaged results.

As Fig. 13 shows, the analysis herein collapses the present data obtained with various α to one E versus Stk trend, however this analysis does not collapse data from other authors onto the same trend at small Stk, where the present data is up to two orders of magnitude smaller than the majority of other researchers. It should be noted that this separation is small compared to the four decade scatter observed at smaller Stk in the literature data, as shown in Fig. 2. The separation between the present results and the previous research is not entirely unexpected, as the conditions of the present study are different from those of previous researchers, with the two most obvious differences being the different shape and flow orientation of the drops, and the different drop fluid, resulting in significantly less drop evaporation. The first difference should be accounted for by Eqs. (14) and (20), however the lower evaporation rate in the present work is not accounted for in this analysis, nor is it captured in Stk. There are also other differences between the present and literature data which are not captured in Fig. 13, such as differences in humidity, d/D, Reynolds, and Schmidt numbers, which are all parameters that appear in models for various scavenging modes (expressions for which are presented in Appendix A), and therefore should have some influence on the measured scavenging. An alternate way to present the data in Fig. 13 is to calculate the model prediction for the conditions of each data point and then compare the predicted and measured result. This allows for a more direct comparison of the data as it accounts for other parameters in addition to Stk. Fig. 14 shows measured E (again, translated to the equivalent spherical value, E_s, using Eqs. (14) and (20)) plotted against the predictions for spherical drop scavenging due to the models presented in the Introduction for the conditions of each data point.

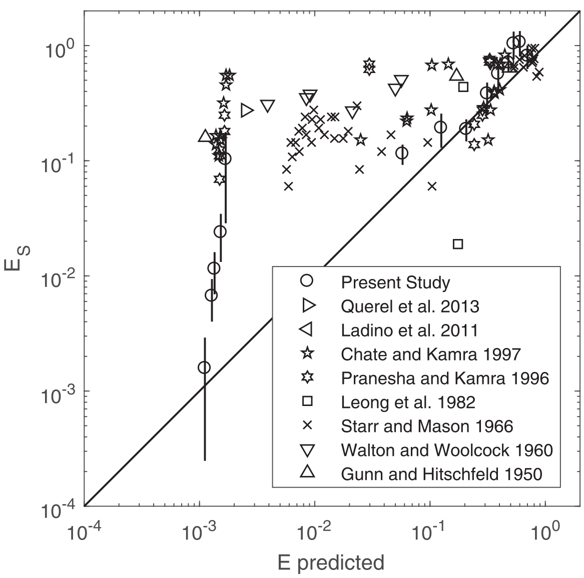

Fig. 14. Plot of measured versus model predicted E for the present results, converted to E_s via Eq. (14) (the vertical lines correspond to 95% confidence intervals), as well as those from the literature surveyed, converted to E_s via Eq. (20). The solid line is of unity slope, and corresponds to exact agreement between the measurements and model prediction.

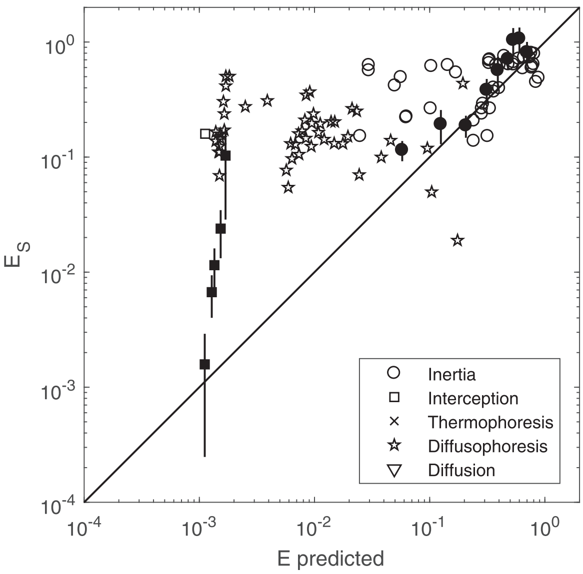

Fig. 15. Plot of measured versus model predicted E for the present results, converted to E_s via Eq. (14) (filled symbols, the vertical lines correspond to 95% confidence intervals), as well as those from the literature surveyed, converted to E_s via Eq. (20) (open symbols). The solid line is of unity slope, and corresponds to exact agreement between measurements and model predictions. The symbols designate the dominant scavenging mechanism for each data point as determined from the model prediction.

As Fig. 14 shows there is generally good agreement between the models and the measurements when E_S is predicted to be greater than 0.1, however as the model predictions for E_S decrease, the models under predict scavenging for a majority of data points. Of note, there is a slightly different behavior exhibited by the present data compared with that of previous researchers when the measured E_S deviates from the model prediction. The literature data shows a nearly horizontal band in Fig. 14, while the present results show a nearly vertical band. To further investigate the source of these discrepancies, the dominant mechanism of each point was identified, and Fig. 14 replotted in Fig. 15 with the symbols identifying the dominant scavenging mechanism of each data point, instead of the author.

Fig. 15 shows that when inertia is dominant the measured scavenging is generally in good agreement with the models, and when inertia is no longer dominant the models no longer predict the measured E well, except for a few points in the present data where interception is dominant. This figure also shows that poor agreement between the models and the literature data occurs when diffusophoresis should be dominant, while the present results are interception dominant when the poor model agreement occurs. To better identify the reason for the deviations, the transition from inertial dominance was investigated. The inertial model has a nearly vertical portion near Stk_*, the critical Stokes number given by: Slinn (1984)

$$Stk_* = \frac{1.2 + \frac{1}{12}\ln(1 + Re)}{1 + \ln(1 + Re)} \tag{24}$$

which defines the lower bound for which inertial scavenging is possible. Near Stk_*, which for the present data is in the range from 0.24 to 0.28, small changes in Stk give large changes in E predicted. The present results with poor model agreement fall just beyond this region of high Stk sensitivity for the inertial contribution to scavenging, and are barely in the interception dominant regime. Several of these points in the present data which show large deviations between the model and measured E are within the measurement uncertainty on Stk of being in this highly Stk sensitive inertially dominant part of the parameter space. This explains the vertical band in the present results seen in Figs. 14 and 15. Given this, we conclude that the present data is in good agreement with the existing models contrary to what is shown in Figs. 14 and 15, which only show the vertical deviation between the measured E and the model predictions, neglecting uncertainty in Stk. This conclusion does not hold for the literature results, however, as when the same amount of uncertainty is applied to Stk for this data there is no similar overlap with the inertial contribution to scavenging. This result can be expected from Figs. 14 and 15 as the data in poor agreement with the models for the literature data here forms a horizontal band instead of a vertical one. This implies that the diffusiophoretic model is under predicting scavenging in this regime. This is consistent with the findings of other researchers who have also noted under prediction in this region (Ardon-Dryer & Huang, 2015; Wang, Zhang, & Moran, 2010; Wang et al., 2011). As the region of largest discrepancy between the present data and the surveyed data occurs in the diffusiophoretic dominant regime it is worth investigating the differences between the present study and studies with water drops further.

The contributions of diffusiophoretic effects on scavenging are dependent on the drop fluid as well as the humidity of the air the drop is falling through, since as the humidity increases the diffusiophoretic contributions will decrease. For water drops to have diffusiophoretic contributions to scavenging not dominant over interception contributions, as is the case for the present results with propylene glycol, the models discussed above require that for a water drop the air must have a relative humidity greater than 95%. For the diffusiophoretic contributions with a water drop to be as small as with the propylene glycol drops used herein, the air would have to have relative humidity of 98%. The highest relative humidity condition in the literature surveyed was that of Querel et al. at 90%, which is still sufficiently low that the diffusiophoretic scavenging is predicted to dominate interception contributions.

This drastic decrease in E in the absence of diffusiophoretic forces can be significant when considering scavenging in rain or sprays, where there is potential for saturation to occur. For rain, saturation will occur at higher altitudes, however there may be large portions of a raindrop's fall time in which it will experience less than saturated air, and therefore the diffusiophoretic contributions will be significant when calculating scavenging. As the duration of a rain event increases, the fraction of a drop's fall time in saturated air will increase as evaporation of previous raindrops will both increase the moisture content of the air and lower the temperature at increasingly lower altitudes. Therefore the time is limited for which appreciable diffusiophoretic contributions to scavenging occurs in a rain event. This phenomena is also applicable to the design of sprays for scavenging in enclosed spaces, as when saturation is reached the performance of the spray will drop.

5. Conclusion

The above work shows that it is possible to perform single drop scavenging experiments using an acoustically levitated droplet to obtain scavenging measurements for a single drop. Using this experimental technique we have demonstrated the following. First, the drop wake has no influence on scavenging both in the attached wake and vortex shedding wake regimes as well as for interception dominated and inertial impaction dominated scavenging regimes. Second, the drop shape has some influence on E at small Stk due to an increase in surface area which can interact with particles, however this shape effect can be accounted for by using the Sauter mean diameter as the characteristic length of the drop when calculating Stk, which allows for the comparison of scavenging for deformed drops in the flow orientation of this experiment. Third, a method was developed to extrapolate the equivalent spherical drop scavenging for a deformed drop in the flow orientation of this experiment as well as in the orientation of rain, allowing for direct comparison of scavenging measurements, as well as the use of scavenging models which presume spherical drops to predict scavenging of deformed drops, like those observed in rain. Finally we have shown that by removing diffusiophoretic contributions from an evaporating drop, E, drops significantly. In the absence of these phoretic effects, experiments agree very well with the inertial model of Slinn.

Appendix A. Scavenging model

The scavenging model used herein is the sum of the scavenging contributions from five scavenging mechanisms:

$$E = E_I + E_i + E_D + E_{dph} + E_{tph} \tag{A.1}$$

where E_I is inertial scavenging, E_i is interception scavenging, E_D is scavenging due to diffusional deposition, E_{dph} is diffusiophoretic scavenging, and E_{tph} is thermophoretic scavenging. Expressions for each of the five terms in Eq. (A.1) are now presented:

Inertial scavenging, E_I, is obtained from the model due to Slinn (1984):

$$E_I = \left(\frac{\rho}{\rho_w}\right)^{1/2} \frac{Stk - Stk_*}{Stk - Stk_* + 2/3} \tag{A.2}$$

where ρ_w is the density of water. Inertial impaction, as described in Eq. (A.2) is only applied when Stk is greater than the critical stokes number, Stk_*, which is:

$$Stk_* = \frac{1.2 + \frac{1}{12}\ln(1 + Re)}{1 + \ln(1 + Re)} \tag{A.3}$$

Interception scavenging, E_i, is modeled from the work of Slinn (1984):

$$E_i = 4\frac{d}{D}\left[\frac{\mu}{\mu_d}\left(1 + 2Re^{1/2}\frac{d}{D}\right)\right] \tag{A.4}$$

where μ_d is the viscosity of the drop.

Diffusion scavenging, E_D is obtained from the work of Slinn (1984):

$$E_D = \frac{4}{ReSc}(1 + 0.4Re^{1/2}Sc^{1/3} + 0.16Re^{1/2}Sc^{1/2}) \tag{A.5}$$

where Sc is the Schmidt number, $Sc = \mu/\rho_a\mathcal{D}$ where $\mathcal{D}$ is the particle diffusion coefficient:

$$\mathcal{D} = \frac{k_b T C_c}{3\pi\mu d} \tag{A.6}$$

where k_b is the Boltzmann constant and T is the air temperature.

Thermophoretic scavenging, E_{tph}, is obtained from the model due to Waldman, as reported by Davenport and Peters (1978):

$$E_{tph} = \frac{4\alpha_{th}(2 + 0.6Re^{1/2}\,Pr^{1/3})(T - T_d)}{UD} \tag{A.7}$$

where T_d is the drop surface temperature, Pr is the Prandtl number of air, and α_{th} is given by:

$$\alpha_{th} = \frac{4C_c\left(k_a + \frac{5\lambda}{D}k_p\right)k_a}{5P\left(1 + \frac{6\lambda}{D}\right)\left(2k_a + k_p + \frac{10\lambda}{D}k_p\right)} \tag{A.8}$$

where k_a and k_p are the air and particle thermal conductivity respectively and P is the air pressure.

Diffusiophoretic scavenging, E_{dph} is obtained from the model due to Waldman and Schmidt as reported by Davenport and Peters (1978):

$$E_{dph} = \frac{4\beta_{dph}(2 + 0.6Re^{1/2}\,Sc_d^{1/3})\left(\frac{P_d^0}{T_d} - \frac{P_a^0\Phi}{T}\right)}{UD} \tag{A.9}$$

where Sc_d is the Schmidt number of the drop vapor diffusing into air, P_d^0 and P_a^0 are the vapor pressure of the drop fluid at the drop surface and air temperature respectively, Φ is the relative humidity of the air, and β_{dph} is given by:

$$\beta_{dph} = \frac{T\mathcal{D}_d}{P}\left(\frac{M_d}{M_a}\right)^{1/2} \tag{A.10}$$

where $\mathcal{D}_d$ is the diffusivity of the drop vapor into air, M_d is the molecular weight of the drop fluid, and M_a is the molecular weight of the air.

Appendix B. Supplementary data

Supplementary data associated with this article can be found in the online version at doi:10.1016/j.jaerosci.2018.10.001.

References

Adams, P. J., & Seinfeld, J. H. (2002). Predicting global aerosol size distributions in general circulation models. *Journal of Geophysical Research, 107* (ACC-4).
Andsager, K., Beard, K. V., & Laird, N. F. (1999). Laboratory measurements of axis ratios for large raindrops. *Journal of the Atmospheric Sciences, 56*, 2673–2683.
Ardon-Dryer, K., Huang, Y.W., & C.D.J. (2015). Laboratory studies of collection efficiency of sub-micrometer aerosol particles by cloud droplets on a single droplet basis, *Atmos. Chem. Phys. Discuss. 15* 6207–6236.
Beard, K. V., & Chuang, C. (1987). A new model for the equilibrium shape of raindrops. *Journal of the Atmospheric Sciences, 44*, 1509–1524.
Beard, K. V., & Grover, S. N. (1974). Numerical collision efficiencies for small raindrops colliding with micron size particles. *Journal of the Atmospheric Sciences, 31*, 543–550.
Beard, K. V., Ochs, H. T., & Kubesh, R. J. (1989). Natural oscillations of small raindrops. *Nature, 342*, 408–410.
Beard, K. V. (1974). Experimental and numerical collision efficiencies for submicron particles scavenged by small raindrops. *Journal of the Atmospheric Sciences, 31*, 1595–1603.
Beard, K. V. (1976). Terminal velocity and shape of cloud and precipitation drops aloft. *Journal of the Atmospheric Sciences, 33*, 851–864.
Bell, J.H., & Mehta, R.D. (1988). Contraction design for small low-speed wind tunnels, *Tech. rep., NASA*.
Berglund, R. N., & Liu, R. Y. H. (1973). Generation of monodisperse aerosol standards. *Environmental Science & Technology, 7*, 147–153.
Byrne, M.A., & J.S.G. (1993). Scavenging of sub-micrometer aerosol particles by water drops, Atmos. Environ. 27A 2099–2105.
Calvert, S., & Englund, H. M. (1984). *Handbook of air pollution technology.* New York: Wiley.
Calvert, S. (1970). Venturi and other atomizing scrubbers efficiency and pressure drop. *AICHE Journal, 16*, 392–396.
Canny, J. (1986). A computational approach to edge detection. *IEEE Transactions on Pattern Analysis and Machine Intelligence, 8*, 679–698.
Chate, D. M., & Kamra, A. K. (1997). Collection efficiencies of large water drops collecting aerosol particles of various densities. *Atmospheric Environment, 31*, 1631–1635.
Clark, W. E., & Whitby, K. T. (1967). Concentration and size distribution measurements of atmospheric aerosols and a test of the theory of self-preserving size distributions. *Journal of Atmospheric Sciences, 24*(*6*), 677–687.
Danilov, S. D., & Mironov, M. A. (2000). Mean force on a small sphere in a sound field in a viscous fluid. *Journal of the Acoustical Society of America, 107*, 143–153.
Davenport, H. M., & Peters, L. K. (1978). Field studies of atmospheric particulate concentration changes during precipitation. *Atmospheric Environment, 12*, 997–1008.
Davis, D. L., Bell, M. L., & Fletcher, T. A. (2002). A look back at the London smog of 1952 and the half century since. *Environmental Health Perspectives, 110*, A734–A735.
Docker, D. W., & Pope, C. A. (1994). Acute respiratory effects of particulate air pollution. *Annual Review of Public Health, 15*, 107–132.
Fredericks, S., & Saylor, J. R. (2016). Parametric investigation of two aerosol scavenging models in the inertial regime. *Journal of Aerosol Science, 101*, 34–42.
Fredericks, S., & Saylor, J. R. (2017). Corrigendum to parametric investigation of two aerosol scavenging models in the inertial regime. *Journal of Aerosol Science, 114*, 342–343.
Friedlander, S. K. (1977). *Smoke, dust, and haze.* New York: Oxford University Press.
Gunn, K., & Hitschfeld, W. (1950). A laboratory investigation of the coalescence between large and small water-drops. *Journal of Meteor, 8*, 7–16.
Hampl, V., & Kerker, M. (1972). Scavenging of aerosol particles by a falling water droplet. Effect of particle size. *Journal of Colloid and Interface Science, 40*, 305–308.
Hampl, V., Kerker, M., Cooke, D. D., & Matijevic, E. (1971). Scavenging of aerosol particles by a falling water droplet. *Journal of the Atmospheric Sciences, 28*, 21211–21221.
Hinds, W. C. (1982). *Aerosol technology: Properties, behavior, and measurement of airborne particles.* New York, NY: Wiley-Interscience.
Horvath, H. (1993). Atmospheric light absorption – A review. *Atmospheric Environment. Part A. General Topics, 27*, 293–317.
Kanakidou, M., Seinfeld, J. H., Pandis, S. N., Barnes, I., Dentener, F. J., Facchini, M. C., ... Wilson, J. (2005). Organic aerosol and global climate modelling: A review. *Atmospheric Chemistry, 5*, 1053–1123.
Karlsen, J. T., & Bruus, H. (2015). Forces acting on a small particle in an acoustical field in a thermoviscous fluid. *Physical Review E, 92* (043010–1 – 043010–22).

King, L. V. (1934). On the acoustic radiation pressure on spheres. *Proceedings of the Royal Society of London Series A-Mathematical and Physical Sciences, 147*(*861*), 212–240.
Ladino, L., Stetzer, O., Hattendorf, B., Günther, D., Croft, B., & Lohmann, U. (2011). Experimental study of collection efficiencies between submicron aerosols and cloud droplets. *Journal of the Atmospheric Sciences, 68*, 1853–1864.
Lai, K. Y., Dayan, N., & Kerker, M. (1978). Scavenging of aerosol particles by a falling water droplet. *Journal of the Atmospheric Sciences, 35*, 674–682.
Lamb, H. (1932). *Hydrodynamics* (6th ed.). Cambridge University Press.
Langmuir, I. (1948). The production of rain by a chain reaction in cumulus clouds at temperatures above freezing. *Journal of Meteorology, 5*, 175–192.
Leong, K. H., Beard, K. V., & Ochs, H. T., III (1982). Laboratory measurements of particle capture by evaporating cloud drops. *Journal of the Atmospheric Sciences, 39*, 1130–1140.
Levich, V. G. (1962). *Physicochemical hydrodynamics.* New Jersey: Prentice-Hall.
Marshall, J. S., & Palmer, W. M. (1948). The distributions of raindrops with size. *Journal of Meteorology, 9*, 327–332.
McFarland, A. R., Gong, H., Muyshondt, A., Wente, W. B., & Anand, N. K. (1997). Aerosol deposition in bends with turbulent flow. *Environment Science Technology, 31*(*12*), 3371–3377.
Merrell, T. M., & Saylor, J. R. (2016). Demisting using an ultrasonic standing wave field. *The Journal of the Acoustical Society of America, 141*, 171–182.
Ohkuma, S., & Poole, B. (1978). Fluorescence probe measurement of the intralysosomal pH in living cells and the perturbation of pH by various agents. *Proceedings of the National Academy of Sciences of the United States of America, 75*, 3327–3331.
Pope, C. A., Thun, M. J., Namboodiri, M. M., Dockery, D. W., Evans, J. S., Speizer, F. E., & Heath, C. W. (1995). Particulate air pollution as a predictor of mortality in a prospective study of U.S. adults. *American Journal of Respiratory and Critical Care Medicine, 151*, 669–674.
Pranesha, T. S., & Kamra, A. K. (1996). Scavenging of aerosol particles by large water drops 1, Neutral case. *Journal of Geophysical Research, 101* (23,373–23,380).
Pruppacher, H., & Klett, J. (1978). *Microphysics of clouds and precipitation.* Dordrecht: Reidel Publishing Company.
Quérel, A., Monier, M., Flossmann, A.I., Lemaitre, P., & Porcheron, E. The importance of new collection efficiency values including the effect of rear capture for the below-cloud scavenging of aerosol particles, *Atmos. Res*.
Ramanathan, V., Crutzen, P. J., Kiehl, J. T., & Rosenfeld, D. (2001). Aerosols, climate, and the hydrological cycle. *Science, 294*, 2119–2124.
Ran, W., Saylor, J. R., & Holt, R. G. (2014). Improved particle scavenging by a combination of ultrasonics and water sprays. *Journal of Aerosol Science, 67*, 104–118.
Roeckner, E., Bäuml, G., Bonaventura, L., Brokopf, R., Esch, M., & Giorgetta, M., et al. (2003). The atmospheric general circulation model ECHAM 5. PART I: Model description, *Tech. rep., MPI für Meteorologie*.
Sakamoto, H., & Haniu, H. (1990). A study on vortex shedding from spheres in a uniform flow. *Journal of Fluids Engineering, 112*, 386–392.
Saylor, J. R., & Jones, B. K. (2005). The existence of vortices in the wakes of simulated raindrops. *Physics of Fluids, 17* (31706–31706)(4).
Saylor, J. R. (1995). Photobleaching of disodium fluorescein in water. *Experiments in Fluids, 18*, 445–447.
Schwartz, J., & Dockery, D. W. (1992). Increased mortality in Philadelphia associated with daily air pollution concentrations. *The American Review of Respiratory Disease, 145*, 600–604.
Schwartz, J., Laden, F., & Zanobetti, A. (2002). The concentration-response relation between PM2.5 and daily deaths. *Environmental Health Perspectives, 110*(*10*), 1025–1029.
Schwartz, J. (1994). What are people dying of on high air pollution days? *Environmental Research, 64*, 26–35.
Seaton, A., MacNee, W., Donaldson, K., & Godden, D. (1995). Particulate air pollution and acute health effects. *The Lancet, 345*, 176–178.
Settnes, M., & Bruus, H. (2012). Forces acting on a small particle in an acoustical field in a viscous fluid. *Physical Review E, 85*(*1*), 016327.
Shen, C. L., Xie, W. J., & Wei, B. (2010a). Parametric resonance in acoustically levitated water drops. *Physics Letters A, 374*(*23*), 2301–2304.
Shen, C. L., Xie, W. J., & Wei, B. (2010b). Parametrically excited sectorial oscillation of liquid drops floating in ultrasound. *Physical Review E, 81*(*4*), 046305.
Slinn, W. G. N., & Hales, J. M. (1971). A reevaluation of the role of thermophoresis as a mechanism of in-and below-cloud scavenging. *Journal of the Atmospheric Sciences, 28*(*8*), 1465–1471.
Slinn, W. G. N. (1984). Precipitation scavenging. *Atmospheric Science and Power Production,* 466–532.
Starr, J. R., & Mason, B. J. (1966). The capture of airborne particles by water drops and simulated snow crystals. *Quarterly Journal of the Royal Meteorological Society, 92*, 490–499.
Tokay, A., & Beard, K. V. (1996). A field study of raindrop oscillations. Part 1: Observation of size spectra and evaluation of oscillation causes. *Journal of Applied Meteorology and Climatology, 35*, 1671–1687.
Trinh, E., & Wang, T. G. (1982). Large-amplitude free and driven drop-shape oscillations: Experimental observations. *Journal of Fluid Mechanics, 122*, 315–338.
Trinh, E. H. (1985). Compact acoustic levitation device for studies in fluid dynamics and material science in the laboratory and microgravity. *Review of Scientific Instruments, 56*, 2059–2065.
Vohl, O., Mitra, S. K., Kiehl, K., & Huber, G. (2001). A wind tunnel study of turbulence effects on the scavenging of aerosol particles by water drops. *Journal of the Atmospheric Sciences, 58*, 3064–3072.
Walton, W. H., & Woolcock, A. (1960). The suppression of airborne dust by water spray. *International Journal of Air Pollution, 3*, 129–153.
Wang, P. K., & Pruppacher, H. R. (1977). Acceleration to terminal velocity of cloud and raindrops. *Journal of Applied Meteorology and Climatology, 16*, 276–280.
Wang, X., Zhang, L., & Moran, M. D. (2010). Uncertainty assessment of current size-resolved parameterizations for below-cloud particle scavenging by rain. *Atmospheric Chemistry, 10*, 5685–5705.
Wang, X., Zhang, L., & Moran, M. D. (2011). On the discrepancies between theoretical and measured below-cloud particle scavenging coefficients for rain-a numerical investigation using a detailed one-dimensional cloud microphysics model. *Atmospheric Chemistry, 11*(*22*), 11859–11866.
Webster, H.N., & Thomson, D.J. (2014). The NAME wet deposition scheme, Tech. rep., Forecasting Res. Tech. Rep.
Zamyshlyaev, A., & Shrager, G. (2004). Fluid flows past spheroids at moderate Reynolds numbers. *Fluid Dynamics, 39*(*3*), 376–383.